



Lack of Adiponectin Drives Hyperosteoclastogenesis in Lipoatrophic Mice

OPEN ACCESS

Edited by:

Natalie A. Sims,
University of Melbourne, Australia

Reviewed by:

Natalie Wee,
University of Melbourne, Australia
Jiake Xu,
University of Western Australia,
Australia

*Correspondence:

Béatrice Desvergne
beatrice.desvergne@unil.ch
David Moulin
david.moulin@univ-lorraine.fr

† These authors have contributed
equally to this work and share first
authorship

*Present address:

Federica Gilardi,
Faculty Unit of Toxicology, CURML,
Faculty of Biology and Medicine,
University of Lausanne, Lausanne,
Switzerland

Specialty section:

This article was submitted to
Cellular Biochemistry,
a section of the journal
Frontiers in Cell and Developmental
Biology

Received: 08 November 2020

Accepted: 22 February 2021

Published: 01 April 2021

Citation:

Madel M-B, Fu H, Pierroz DD,
Schiffirin M, Winkler C, Wilson A,
Pochon C, Toffoli B, Taïeb M,
Jouzeau J-Y, Gilardi F, Ferrari S,
Bonnet N, Blin-Wakkach C,
Desvergne B and Moulin D (2021)
Lack of Adiponectin Drives
Hyperosteoclastogenesis in
Lipoatrophic Mice.
Front. Cell Dev. Biol. 9:627153.
doi: 10.3389/fcell.2021.627153

Maria-Bernadette Madel^{1†}, He Fu^{2†}, Dominique D. Pierroz³, Mariano Schiffirin², Carine Winkler², Anne Wilson⁴, Cécile Pochon⁵, Barbara Toffoli², Mahdia Taïeb¹, Jean-Yves Jouzeau⁵, Federica Gilardi^{2†}, Serge Ferrari⁶, Nicolas Bonnet⁷, Claudine Blin-Wakkach¹, Béatrice Desvergne^{2*} and David Moulin^{5*}

¹ Université Côte d'Azur, CNRS, UMR 7370, Laboratoire de Physiologie Moléculaire, Nice, France, ² Center for Integrative Genomics, Genopode, Lausanne Faculty of Biology and Medicine, Lausanne, Switzerland, ³ International Osteoporosis Foundation, Nyon, Switzerland, ⁴ Department of Oncology, University of Lausanne, Epalinges, Switzerland, ⁵ Université de Lorraine, CNRS, IMoPA, Nancy, France, ⁶ Division of Bone Diseases, Department of Internal Medicine Specialties, Geneva University Hospital, Faculty of Medicine, Geneva, Switzerland, ⁷ Nestlé Research, Lausanne, Switzerland

Long bones from mammals host blood cell formation and contain multiple cell types, including adipocytes. Physiological functions of bone marrow adipocytes are poorly documented. Herein, we used adipocyte-deficient PPAR γ -whole body null mice to investigate the consequence of total adipocyte deficiency on bone homeostasis in mice. We first highlighted the dual bone phenotype of PPAR γ null mice: on the one hand, the increased bone formation and subsequent trabecularization extending in the long bone diaphysis, due to the well-known impact of PPAR γ deficiency on osteoblasts formation and activity; on the other hand, an increased osteoclastogenesis in the cortical bone. We then further explored the cause of this unexpected increased osteoclastogenesis using two independent models of lipoatrophy, which recapitulated this phenotype. This demonstrates that hyperosteoclastogenesis is not intrinsically linked to PPAR γ deficiency, but is a consequence of the total lipodystrophy. We further showed that adiponectin, a cytokine produced by adipocytes and mesenchymal stromal cells is a potent inhibitor of osteoclastogenesis *in vitro* and *in vivo*. Moreover, pharmacological activation of adiponectin receptors by the synthetic agonist AdipoRon inhibited mature osteoclast activity both in mouse and human cells by blocking podosome formation through AMPK activation. Finally, we demonstrated that AdipoRon treatment blocks bone erosion *in vivo* in a murine model of inflammatory bone loss, providing potential new approaches to treat osteoporosis.

Keywords: adiponectin, osteoclast, bone marrow adiposity, cortical bone porosity, AMPK

INTRODUCTION

Bone homeostasis is a result of constant remodeling activities, with a balance of bone resorption and bone formation. The most prevalent disorder of bone homeostasis is osteoporosis, affecting men and women, with a particular high prevalence in post-menopausal women. The low efficacy of actual anti-osteoporotic therapeutic options highlights the need of better understanding the pathophysiological processes at work.

The role of adipocyte in bone homeostasis is one of the factors raising great interest, but it faces quite some complexity. An illustration of this complexity is the fact that obesity is traditionally considered to be protective against osteoporosis, consequently to an increased proliferation and differentiation of osteoblasts and osteocytes stimulated by mechanical load (Felson et al., 1993). However, obesity in post-menopausal women and in men correlates with increased marrow adiposity, alteration of the bone microarchitecture, and increased risk of fracture (Sheu and Cauley, 2011). Thus, the respective roles of aging, increased BMI, and visceral *vs.* bone marrow fat on bone homeostasis remain difficult to disentangle (Horowitz et al., 2017; Cornish et al., 2018).

Peroxisome proliferator-activated receptors (PPARs) are ligand-activated transcription factors that belong to the nuclear hormone receptor superfamily. PPAR γ is a key factor and master regulator in adipocytes development and functions (Tontonoz and Spiegelman, 2008). Indeed, loss-of-function studies both *in vitro* and *in vivo* have clearly demonstrated that PPAR γ is essential for the formation of adipose tissue (Barak et al., 1999; Rosen et al., 1999; Wang et al., 2013) and mature adipocyte homeostasis (Imai et al., 2004). Recently, we demonstrated that mice carrying a full body deletion of PPAR γ (*Pparg* $^{\Delta/\Delta}$) are totally devoid of adipocytes (Sardella et al., 2018). The activity of PPAR γ is also central in bone homeostasis by modulating both bone formation by osteoblasts and bone resorption due to osteoclast activity. First, adipocytes and osteoblasts share same mesenchymal progenitors, and the cell fate decision between adipocyte and osteoblast lineages depends on various signals (Idris et al., 2009; Calo et al., 2010; Kawai and Rosen, 2010; Wan, 2010). Activation of PPAR γ inhibits osteoblast formation, and thus bone formation, by favoring adipocyte differentiation (Rzonca et al., 2004; Ali et al., 2005). Along this line, *in vivo* evidence indicates that mice heterozygous for a null allele of the gene encoding PPAR γ (*Pparg*) exhibit increased osteoblastogenesis, which results in increased bone mass with a doubling of the rate of new bone formation, when compared to control mice. Moreover, PPAR γ also directly inhibits osteoblast activity, independently of osteoblast-specific *Pparg* deletion in osteoblast differentiation and trabecular bone formation (Sun et al., 2013). Second, in bone resorption, PPAR γ promotes osteoclastogenesis, as illustrated by increased osteoclast numbers in aged mice treated with thiazolidinediones, which are high-affinity synthetic PPAR γ agonists (Lazarenko et al., 2007). Conversely, mice in which *Pparg* is specifically deleted in endothelial and hematopoietic cells (i.e., affecting osteoclast progenitors but not osteoblasts), exhibit decreased osteoclastogenesis compared to wild-type mice, provoking osteopetrosis with impaired bone resorption and reduced medullary cavities (Wan et al., 2007). However, a recent controversy on the role of PPAR γ in osteoclast was raised by Zou et al. who found that only the pharmacological, and not the physiological activation of PPAR γ affects osteoclastogenesis (Zou et al., 2016). Finally, hyperactivation of PPAR γ via agonist treatment causes accumulation of adipocytes in the bone marrow in thiazolidinedione-treated rodents, whereas

increased bone loss and bone fractures have been correlated with thiazolidinedione therapy in humans (Lazarenko et al., 2007; Grey, 2008; Kahn et al., 2008).

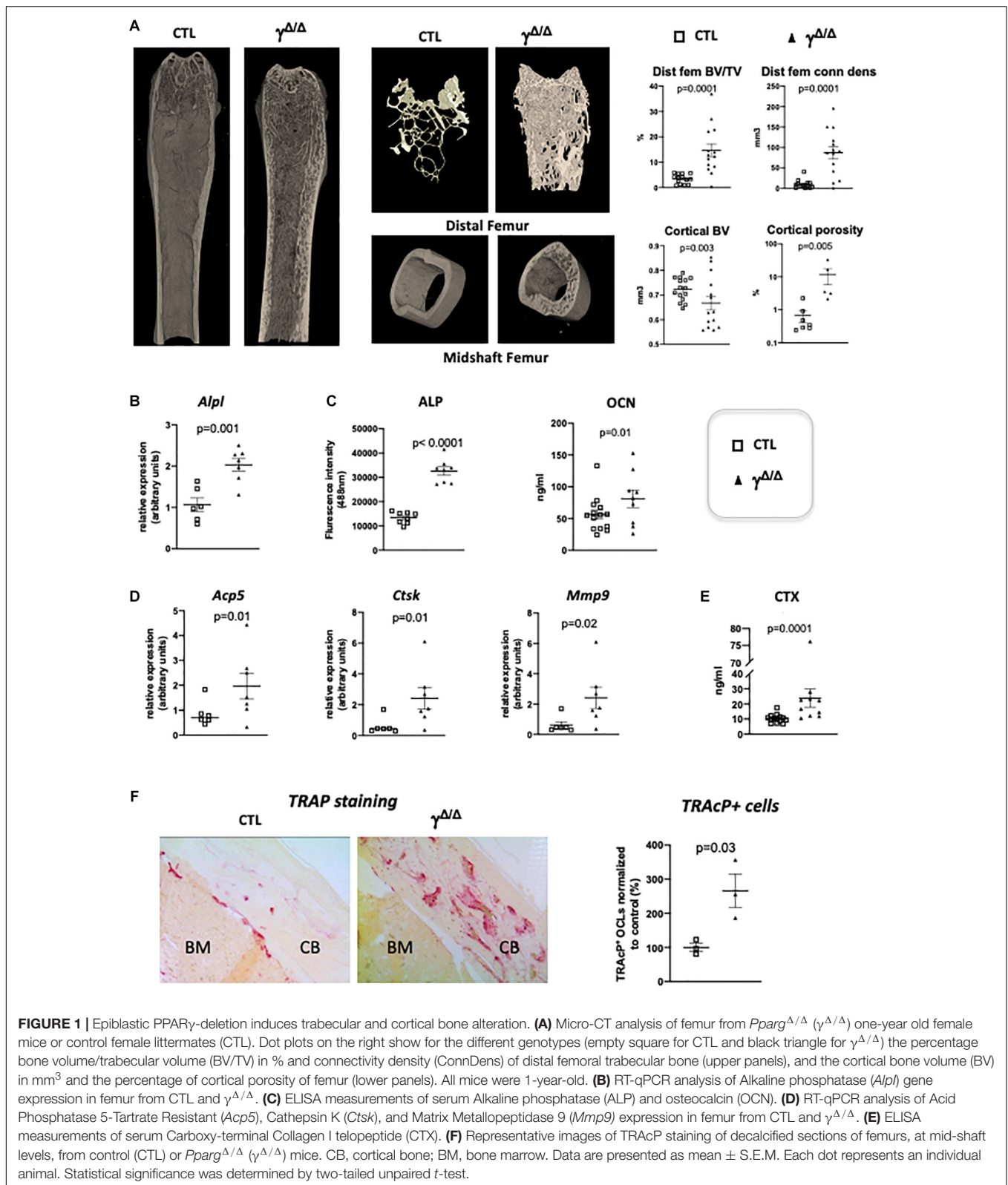
Herein, we used mice carrying a PPAR γ full body deletion to explore the consequences of the lack of adipocyte on bone homeostasis, and demonstrate that as expected, there is a strong increased bone density of the trabecular bone. However, this phenotype was associated with an exacerbated osteoclastogenesis. Using two other complementary models of genetically-induced lipotrophic mice, *i.e.* mice carrying an adipose-tissue specific deletion of PPAR γ and AZIP mice, we then further explore the cross-talk between adipocytes and osteoclasts, whose alteration leads to hyperosteoclastogenesis and osteoporosis.

RESULTS

In order to evaluate the impact of adipose tissue on bone homeostasis, we studied lipotrophic mice, that we recently generated. These mice, hereby called *Pparg* $^{\Delta/\Delta}$ carry a whole body deletion of PPAR γ and were obtained through epiblastic (Sox2 promoter) *cre* deletion of the *Pparg* allele (Sardella et al., 2018). Bone analyses of female one-year-old mice first showed that these mice displayed dramatic alterations of both trabecular and cortical bones (**Figure 1**). The three-dimensional images generated by trabecular bone microcomputed tomography (3D micro-CT) reconstruction of the femurs of one-year old female mice highlighted a remarkably high trabecularization of the bone architecture in *Pparg* $^{\Delta/\Delta}$ mice, which extended along the shaft and almost reached the mid-diaphysis (**Supplementary Video S1, Figures 1A, and Table 1A**). In contrast, the cortical bone was found to be extremely porous at the epiphysis and the diaphysis. Owing to hypertrabecularization and high cortical porosity, the frontier between these two types of bone along the diaphysis remained difficult to establish. The phenotype was also observed in *Pparg* $^{\Delta/\Delta}$ male mice. However, the difficulties to obtain an appropriate number of old *Pparg* $^{\Delta/\Delta}$ males (due to premature death, still being investigated), and the fact that old female mice had a marked phenotype lead us to pursue all further explorations in females.

We first further evaluated in female whether the bone alterations appear during development or appear progressively with age, by performing micro CT measurements at 5–6 months. A quantification of the diverse parameters is shown in **Table 1B**. More particularly, we found that the increased trabecular number and connectivity density in both vertebral bodies and distal femoral metaphysic bones appeared at 5–6 months of age, whereas the alteration of cortical parameters were only seen in 1 year-old mice.

Molecular analyses confirmed an increased trabecular bone formation, as exemplified by increased levels of alkaline phosphatase mRNA (*Alp1*) in the bone, evaluated by RT-qPCR and increased levels of alkaline phosphatase (ALP) and osteocalcin (OCN) in the serum measured by ELISA (**Figures 1B,C**). To evaluate whether osteocytes, which come from osteoblasts and are mature permanent bone cells, *versus* osteoblast populations were altered in these mice,



we measured the mRNA levels of sclerostin (*Sost*) and keratan (*Kera*), which are expressed by osteocytes and osteoblasts, respectively (Jilka et al., 2014). Both markers were

unchanged (**Supplementary Figure S1**). Three-D micro-CT of the fourth lumbar vertebrae clearly demonstrated increased trabecular bone volume fraction and trabecular connectivity

TABLE 1 | (A) Micro-CT data were obtained from various bones in *Pparg*^{fl/+} and *Pparg*^{Δ/Δ} of 1 year-old female mice. **(B)** Similar evaluation of bones from 5/6 month-old female mice.

A. Micro CT analyses of 1 year-old female mice		
1 year	<i>Pparg</i> ^{fl/+}	<i>Pparg</i> ^{Δ/Δ}
No. of animals assessed	15	14
Cortical TV (mm ³)	1.498 ± 0.023	1.327 ± 0.031*
Cortical BV (mm ³)	0.723 ± 0.012	0.667 ± 0.028*
Cortical thickness (μm)	241.8 ± 4.5	208.0 ± 10.4*
Dist femoral BV/TV (%)	3.41 ± 0.49	14.38 ± 2.26*
Dist femoral conn density (mm ³)	9.18 ± 2.57	81.89 ± 13.62*
Dist femoral Tb N (/mm)	2.39 ± 0.09	3.61 ± 0.22*
Dist femoral Tb Th (μm)	54.37 ± 2.48	57.28 ± 3.52*
Dist femoral Tb Sp (μm)	431.34 ± 18.4	291.10 ± 9.70*
Vertebral BV/TV (%)	17.33 ± 1.38	29.57 ± 3.30*
Vertebral conn density (mm ³)	127.02 ± 14.89	519.44 ± 73.33*
Vertebral Tb N (/mm)	3.42 ± 0.17	6.29 ± 0.53*
Vertebral Tb Th (μm)	51.43 ± 1.88	47.04 ± 2.30
Vertebral Tb Sp (μm)	311.13 ± 16.23	177.30 ± 15.73*
B. Complete bone analysis by micro CT of 5/6 month-old female mice		
5–6 months	<i>Pparg</i> ^{fl/+}	<i>Pparg</i> ^{Δ/Δ}
No. of animals assessed	8	10
Cortical TV (mm ³)	1.18 ± 0.05	1.18 ± 0.04
Cortical BV (mm ³)	0.0541 ± 0.023	0.0548 ± 0.014
Cortical thickness (μm)	203.75 ± 4.80	202.80 ± 5.33
Dist femoral BV/TV (%)	7.78 ± 1.17	8.55 ± 1.07
Dist femoral conn density (mm ³)	38.90 ± 8.70	84.30 ± 14.85*
Dist femoral Tb N (/mm)	3.13 ± 0.13	3.75 ± 0.22*
Dist femoral Tb Th (μm)	53.01 ± 1.62	45.93 ± 2.24*
Dist femoral Tb Sp (μm)	327.46 ± 15.03	283.59 ± 21.33
Vertebral BV/TV (%)	15.49 ± 1.31	21.44 ± 1.79*
Vertebral conn density (mm ³)	112.73 ± 12.56	275.53 ± 33.10*
Vertebral Tb N (/mm)	3.71 ± 0.13	4.76 ± 0.17*
Vertebral Tb Th (μm)	49.03 ± 1.17	46.39 ± 1.14
Vertebral Tb Sp (μm)	278.37 ± 10.66	215.1 ± 8.32*

Values are given as mean ± standard deviation. TV, total volume; BV, bone volume; Tb N, trabecular number; Tb Th, trabecular thickness; Tb Sp, trabecular separation. **p* < 0.05 vs. *Pparg*^{fl/+}.

density, indicating increased osteoblastogenesis in *Pparg*^{Δ/Δ} (Supplementary Figure S1), in agreement with previous report (Akune et al., 2004). These results are consistent with the pivotal role of PPARγ on the fate of bone marrow mesenchymal stromal cells, with previous reports showing increased osteoblastogenesis when PPARγ signaling is pharmacologically or genetically blocked (Takada et al., 2009). As mentioned above, the role of PPARγ in osteoblastogenesis has been well documented and was therefore not further investigated in the present report.

Remarkably, the expression of bone resorbing markers such as the Tartrate-Resistant Acid Phosphatase Type 5 (*Acp5*), cathepsin K (*Ctsk*) was increased in the long bones of *Pparg*^{Δ/Δ} mice compared to control mice. *Mmp9*, which is a key proteinase involved in the recruitment and activity of osteoclasts and endothelial cells for the development of long bones, particularly

in the diaphysis core (Jemtland et al., 1998; Engsig et al., 2000), was also increased (Figure 1D) suggesting an increase in osteoclastogenesis. This is further supported by an augmentation of serum levels of carboxy-terminal collagen I telopeptide (CTX) (Figure 1E). Indeed, TRAcP staining on femoral sections (Figure 1F) confirmed the increased presence of bone-resorbing osteoclasts explaining the observed cortical porosity.

PPARγ is known to play a role in activating osteoclastogenesis. Wan et al. (2007) used a Tie2Cre-directed *Pparg* deletion, which specifically target endothelial cells among which the myeloid-lineage cells —from which the osteoclast is derived. These authors show that this cell-specific *Pparg* deletion severely impaired osteoclastogenesis, whereas PPARγ synthetic agonists exacerbated it (Wan et al., 2007). This role of *Pparg* in osteoclast has been recently questioned by the study of Zou et al. (2016), showing that the *in vivo* effect of PPARγ on osteoclast formation is only seen upon pharmacological activation of PPARγ but neither on physiological nor on pathological osteoclast formation. This raised the question whether the elevated osteoclast activity observed in cortical bone is attributable to lipodystrophy, or to unforeseen intrinsic effects of PPARγ deficiency in the osteoclast lineage. To disentangle these two possibilities, we used another PPARγ-independent lipodystrophic mouse model. *AZIP*^{tg/+} mouse is a hemizygote transgenic mouse strain in which a dominant negative protein of key B-ZIP transcription factors (A-ZIP) blocks adipocyte development. *AZIP*^{tg/+} mice are born with no white adipose tissue and markedly decreased brown adipose tissue (Moitra et al., 1998). In support of the lipodystrophy hypothesis, micro-CT analyses of the femur of 1 year old female *AZIP*^{tg/+} mice revealed an increased cortical porosity (Figure 2A). As observed in *Pparg*^{Δ/Δ} mice, TRAcP staining of longitudinal bone sections revealed increased osteoclast numbers (Figure 2B), further confirmed by the increased expression levels of the osteoclastogenesis markers (Figure 2C). Finally, we generated a third mouse model by invalidating *Pparg* in adipose tissue (*Adipoq*^{cre} *Pparg* fl/fl, *γ*^{FatKO} (Wang et al., 2013), called herein *Pparg*^{adipoKO}). These mice are lipodystrophic, but in contrast to *Pparg*^{Δ/Δ}, they have an unaltered hematopoietic lineage. Here again, micro-CT analysis and osteoclastogenesis markers in one-year old females revealed increased osteoclast numbers and activity with an enhanced cortical porosity, as observed in *Pparg*^{Δ/Δ} mice (Figures 2D,E). These two independent mouse models confirmed that adipocyte deficiency is pivotal to the cortical bone phenotype and the increased osteoclast number observed here.

One consequence of lipodystrophy observed in all three models is a severe type 2 diabetes with signs of diabetic nephropathy (Moitra et al., 1998; Toffoli et al., 2017; Wang et al., 2013). Given that chronic kidney diseases are often accompanied by hyperparathyroidism and result in complex, combined catabolic and anabolic activities in the bones (Levin et al., 2007), we evaluated parathyroid hormone (PTH) levels. As shown in Supplementary Figure S2, no statistically significant differences were observed between *Pparg*^{Δ/Δ} mice and their control littermates in either the circulating levels of PTH or the mRNA levels of the PTH receptor *Pth1r* in the bones or kidneys.

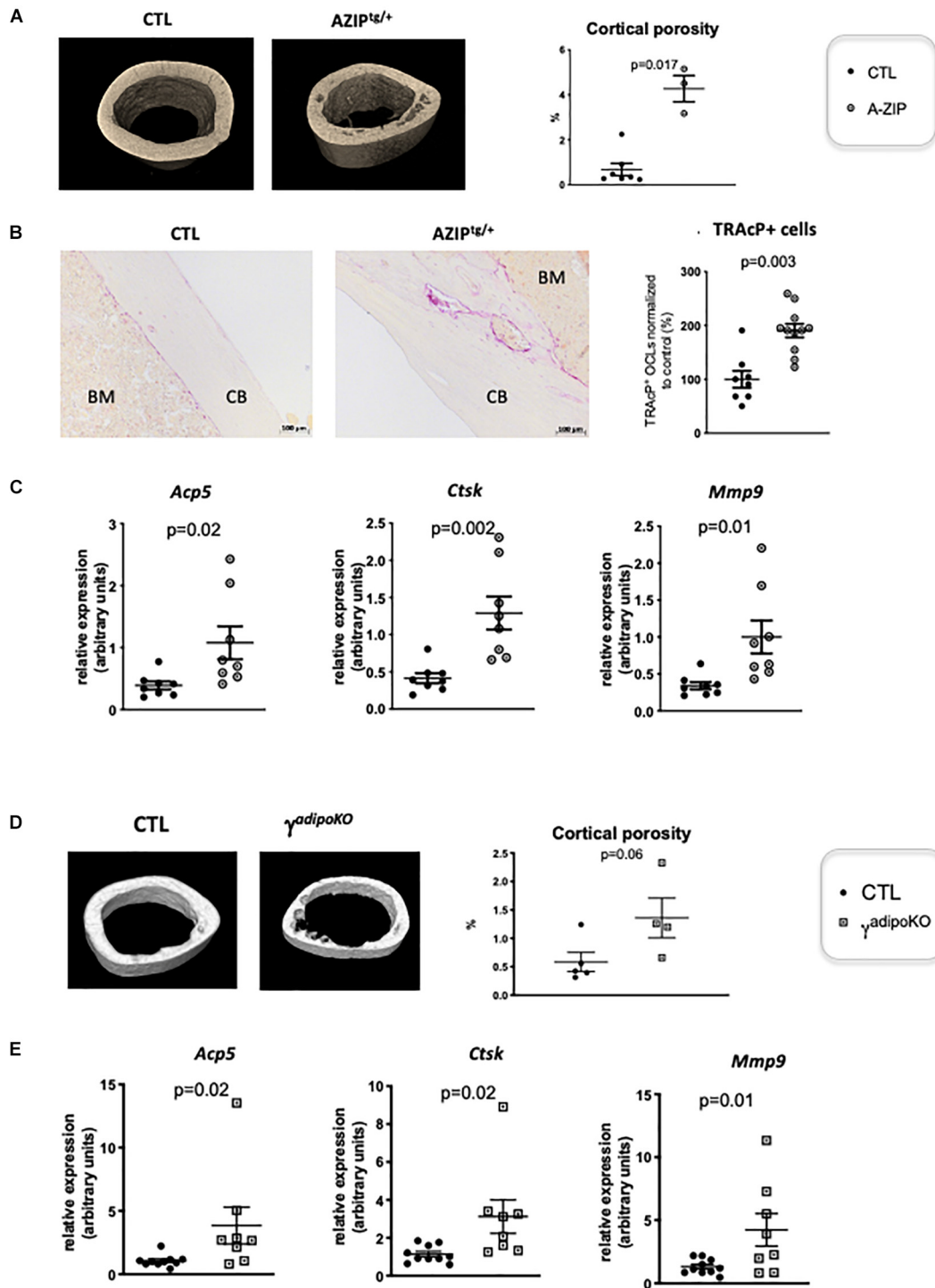


FIGURE 2 | Lipoatrophy is responsible for unregulated osteoclastogenesis. **(A)** Representative 3D sections of midshaft femur from 1 year-old female A-ZIP^{tg/+} and CTL littermates (left panels) and femoral cortical porosity measured by micro-CT analysis of femur from A-ZIP^{tg/+} and control (CTL) littermates (right panel). **(B)** Representative images of TRAcP staining of longitudinal sections of decalcified femurs, at mid-shaft levels, from control (CTL) or A-ZIP^{tg/+} mice (left panels; CB, cortical bone; BM, bone marrow). The right panel is a quantification of TRAcP positive osteoclasts. **(C)** RT-qPCR analysis of Acid Phosphatase 5-Tartrate Resistant (*Acp5*) Cathepsin K (*Ctsk*) and Matrix Metalloproteinase 9 (*Mmp9*) expression in femur from A-ZIP^{tg/+} mice and their control littermates. **(D)** Representative 3D sections of midshaft femur from 1 year-old females PPAR γ ^{adipoKO} and CTL littermates (left panels) and femoral cortical porosity measured by micro-CT analysis of femur from PPAR γ ^{adipoKO} and control (CTL) littermates (right panel). **(E)** RT-qPCR analysis of Acid Phosphatase 5-Tartrate Resistant (*Acp5*) Cathepsin K (*Ctsk*) and Matrix Metalloproteinase 9 (*Mmp9*) expression in femur from PPAR γ ^{adipoKO} mice and their control littermates. Each dot represents an individual animal. Statistical significance was determined by two-tailed unpaired *t*-test.

Notably, serum PTH levels were also unchanged in AZIP^{tg/+} mice (**Supplementary Figure S2**), suggesting that the PTH pathway is unlikely to support the increased bone remodeling observed in lipodystrophic mice.

To investigate how adipocytes regulate osteoclastogenesis, and to evaluate whether factors produced by adipocytes within the bone marrow can influence osteoclastogenesis, we performed an osteoclastogenesis assay using bone marrow cells from wild-type mice cultured in the presence of either control medium (CTL in **Figure 3**) or adipocyte-conditioned medium (ACM) (see **Figure 3A** for a graphic summary of the experiment). Adipocyte-conditioned medium was isolated from culture of adipocyte-differentiated 3T3-L1 cells whereas control medium was obtained from cultures of undifferentiated pre-adipocytes 3T3-L1 cells. The presence in bone marrow cells culture of adipocyte-conditioned medium, compared to pre-adipocyte-conditioned medium, provoked a substantial decrease in the number of mature osteoclasts (**Figure 3B**). Consistently, adipocyte-conditioned medium significantly inhibited bone resorption as assessed by the decrease number of resorption pits in the calvaria resorption assay (**Figure 3C**). These data demonstrate that adipocyte-secreted mediators are responsible for the inhibition of RANKL-induced osteoclast differentiation *in vitro*.

Next, we searched for component(s) of ACM responsible for this anti-osteoclastogenic activity. Interestingly, the ACM inhibitory activity was maintained after filtering out all components larger than 35 kDa from the conditioned medium. The molecular weights of the major adipokines, adiponectin and leptin, are below 35 kDa and their circulating levels are not or barely detectable in *Pparg*^{Δ/Δ} mice, as we previously demonstrated (Gilardi et al., 2019). As expected, the gene expression levels of *Leptin* and *Adiponectin* in long bones of *Pparg*^{Δ/Δ} mice as well as AZIP^{tg/+} mice were extremely low (**Supplementary Figure S3**). Unlike *Leptin*, *Adiponectin* is preferentially expressed by adipocyte and by bone-marrow MSC, and is a well-characterized target gene of *Pparγ* (Iwaki et al., 2003). Western-blot analyses confirmed that adiponectin was present in large amounts in ACM but not in CTL medium (**Figure 3D**). We therefore tested whether blocking adiponectin would affect ACM-mediated inhibition of osteoclastogenesis *in vitro*. As shown in **Figure 3B**, the addition of a blocking adiponectin antibody reversed the reduction in osteoclast number in a dose-dependent manner. These results support that the soluble factors secreted by adipocytes, in particular adiponectin, are inhibitors of osteoclastogenesis. Consistently, the total lack of adipocytes, including in the bone marrow, results in a complete absence of this adipokine, leading to the loss of its repressive activity in osteoclast differentiation.

AdipoRon is a non-peptidic agonist of adiponectin receptors (Okada-Iwabu et al., 2013). We thus perform the reverse experiment of the antibody blocking assay, adding AdipoRon to culture of bone marrow cells. Consistently, AdipoRon recapitulated the blocking effect of ACM on osteoclast differentiation irrespective of the origin of the osteoclast progenitors (bone marrow, spleen, or monocytic-enriched

fraction) with IC50 in the micromolar range (**Figures 4A,B** and **Supplementary Figure S4**). Furthermore, AdipoRon blocked osteoclast differentiation in *Pparγ* deficient cells, confirming that intrinsic PPAR γ alterations do not play a role in the observed phenotype (**Figure 4C**).

Previous studies demonstrated *in vivo* that mice treated with adiponectin expressing adenovirus have reduced osteoclast numbers and bone-resorption markers (Oshima et al., 2005). Using the macrophage cell line RAW264, prone to differentiate in osteoclasts, these authors further showed that adiponectin blocked *in vitro* osteoclastogenesis by inhibiting NFATc1. Blockade of NFATc1 was suggested to occur through activation of the AMPK signaling pathway, a key integrator of metabolic signals and target of adiponectin signaling (Yamaguchi et al., 2008). We thus tested whether this mechanism would apply *in vivo* and to primary cells. Flow cytometry analysis combining nuclei staining (Madel et al., 2018) and anti-AdipoR1 antibody, confirmed that the adiponectin receptor AdipoR1 is expressed also by mature osteoclasts generated from murine bone marrow cells (**Figure 4D**). Furthermore, RT-PCR performed on osteoclasts from different origins (bone marrow, bone marrow-derived dendritic cells, bone marrow monocytic cells) showed that osteoclasts express both adiponectin receptors AdipoR1 and AdipoR2 (**Figure 4E**). In agreement, western-blot analysis of AMPK phosphorylation confirmed that the Adiponectin signaling pathway is active in both precursors and mature osteoclasts sorted on the basis of their nuclei number (≥ 3) (Madel et al., 2018; **Figures 4F-H**).

AdipoRon was thus used to investigate the consequences of adiponectin receptor activation on murine and human osteoclasts. AICAR was used as a synthetic activator of AMPK. As seen in **Figures 5A,B** each of these molecules inhibited the formation of podosomes that are essential for bone resorption. Moreover, dorsomorphin, a reversible AMP-kinase inhibitor, could reverse the AdipoRon inhibitory effect (**Figure 5B**). This is in line with the recently published effect of recombinant adiponectin on RAW264.7 cells, confirming the impact of adiponectin on both osteoclasts differentiation and podosome formation (Chen et al., 2018) and endorsing the use of AdipoRon as a surrogate activator for adiponectin receptors. Finally, adiponectin signaling regulates numerous cellular metabolic pathways including mitochondrial functions (Iwabu et al., 2010). AdipoRon treatment provoked disruption of the perinuclear mitochondrial network when added to culture of mature osteoclasts (**Figure 5C**). Altogether, these results indicate that, beside its inhibiting action in osteoclast differentiation, adiponectin signaling exerts a pivotal role in mature osteoclast energy homeostasis regulation.

The inhibitory effect of AdipoRon was further tested *in vivo* on the well-described model of osteoclast bone resorption induced by lipopolysaccharide (LPS) injection into the mouse calvaria. Both micro-CT and TRAcP staining (**Figure 5D**) showed that AdipoRon administration resulted in a strong decrease in osteoclast numbers and bone resorption pits on calvaria.

We thus aimed to validate our findings on human cells and therefore investigated the impact of AdipoRon on hPBMC-derived osteoclasts. Consistent with the results

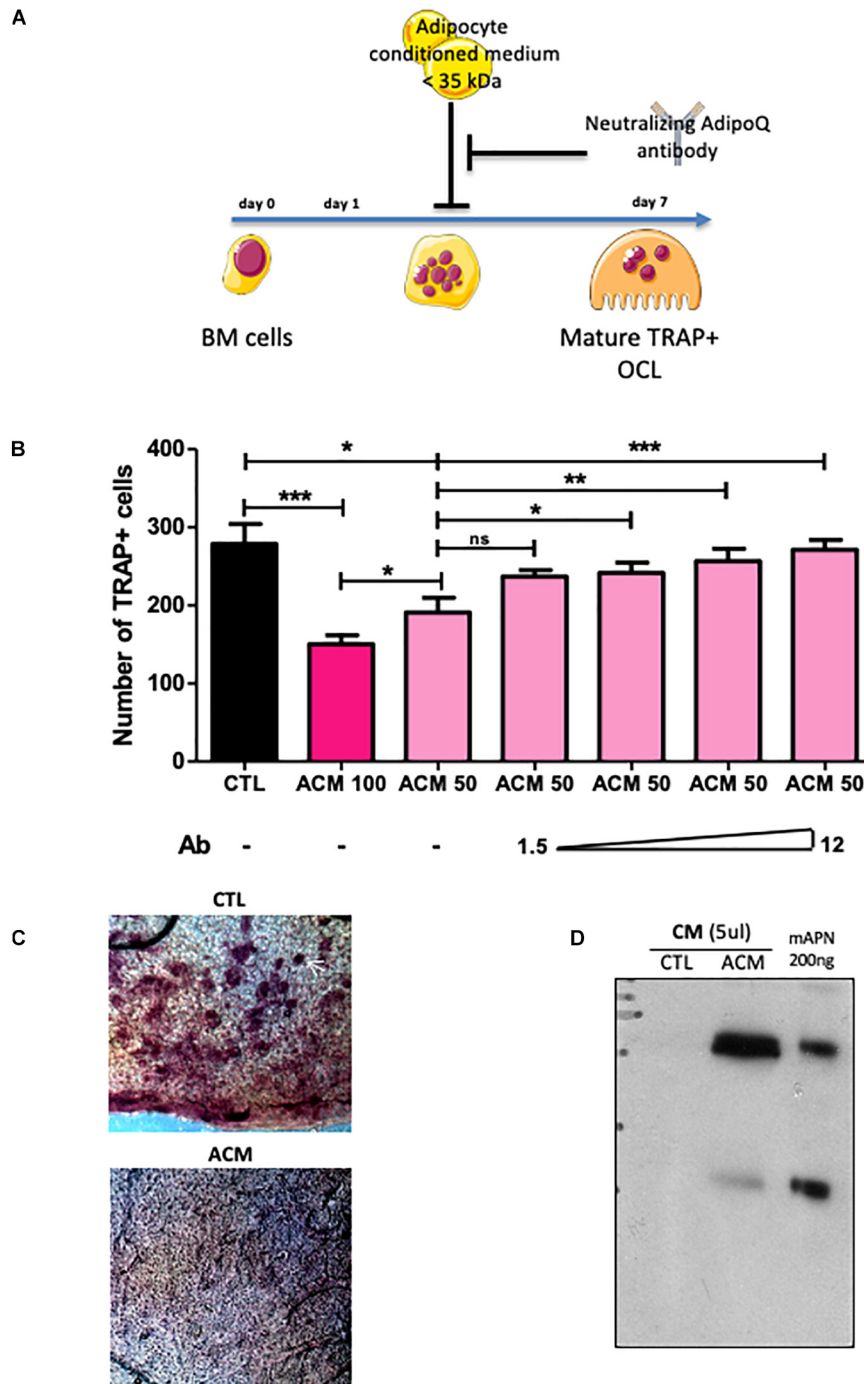
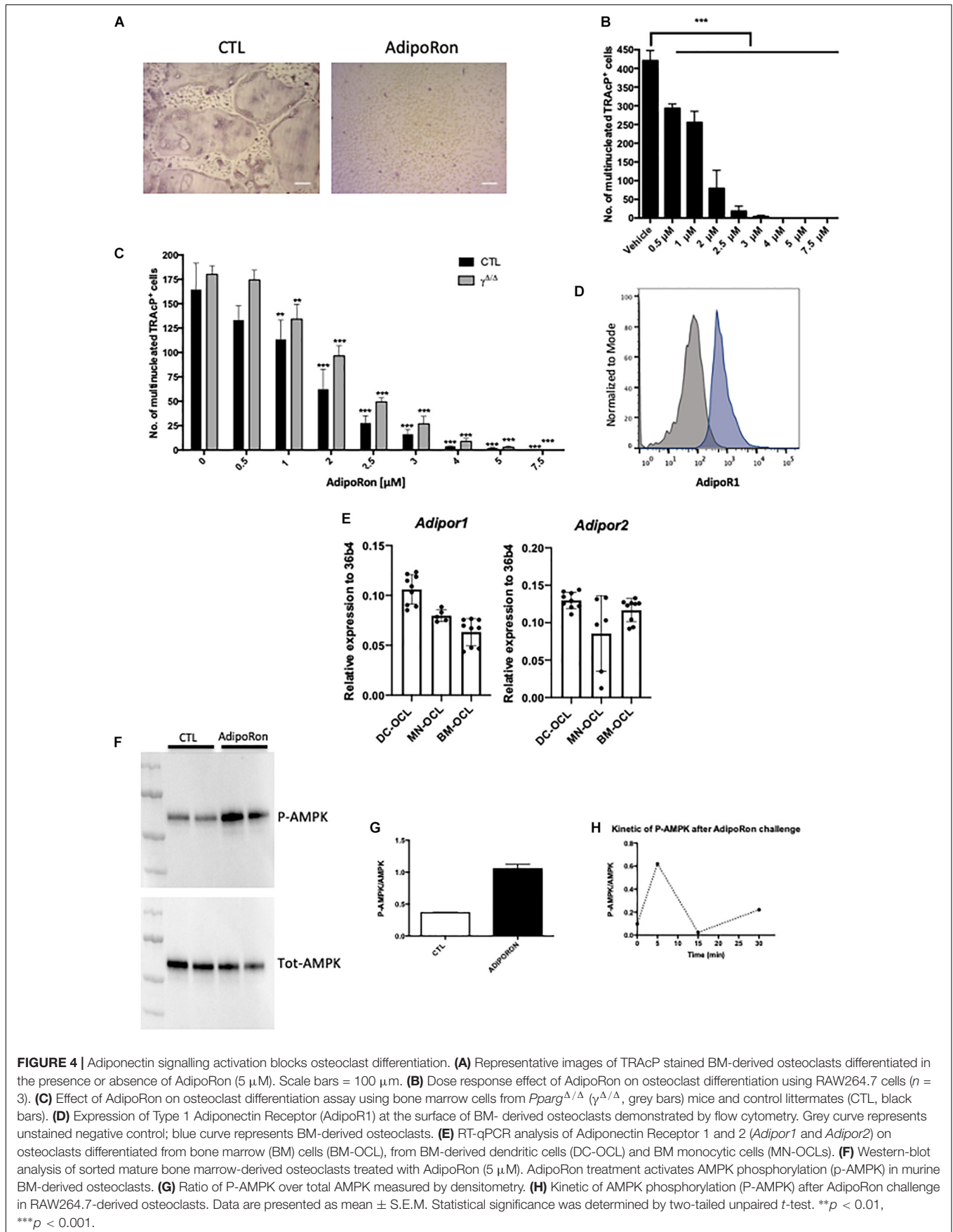


FIGURE 3 | Adipocyte conditioned medium inhibits osteoclastogenesis. **(A)** Experimental design of the *in vitro* assay used to test anti-osteoclastogenic activity from mature adipocyte secreted factors. **(B)** One day after plating, wild type BM cells were cultured for 6 more days in the presence of M-CSF and RANKL (osteoclast differentiation media) in addition to conditioned medium prepared from differentiated (ACM, adipocyte-conditioned medium) or undifferentiated (CTL: control-conditioned medium) 3T3-L1 preadipocytes. Different doses of a specific blocking antibody against adiponectin (1.5–12.0 $\mu\text{g}/\text{ml}$) were added to the conditioned medium (ACM50) during osteoclast differentiation (ACM 100 means pure ACM; ACM50 means 1:1 diluted ACM with osteoclast differentiation medium). Data are presented as mean \pm SEM of biological triplicates. Statistical significance was determined by two-tailed unpaired *t*-test. * $p < 0.05$, ** $p < 0.01$, *** $p < 0.001$. **(C)** Calvaria resorption pit assay. Representative sections of skulls from 14 day-old wild-type pups cultured for 2 weeks in complete α MEM in the presence of conditioned medium from either undifferentiated 3T3-L1 preadipocytes (CTL, $n = 3$) or mature 3T3-L1 adipocytes (ACM, $n = 3$), after TRAP staining. Top panel: the white arrow indicates one example of resorption pit seen in many places on the skull with CTL medium, while absent with the ACM culture medium. **(D)** Western-blot analysis of conditioned medium from undifferentiated (CTL) and differentiated 3T3-L1 adipocyte (A-CM) against adiponectin. Recombinant mouse adiponectin (200 ng rmAdiponectin) was added to demonstrate specificity of the signal.



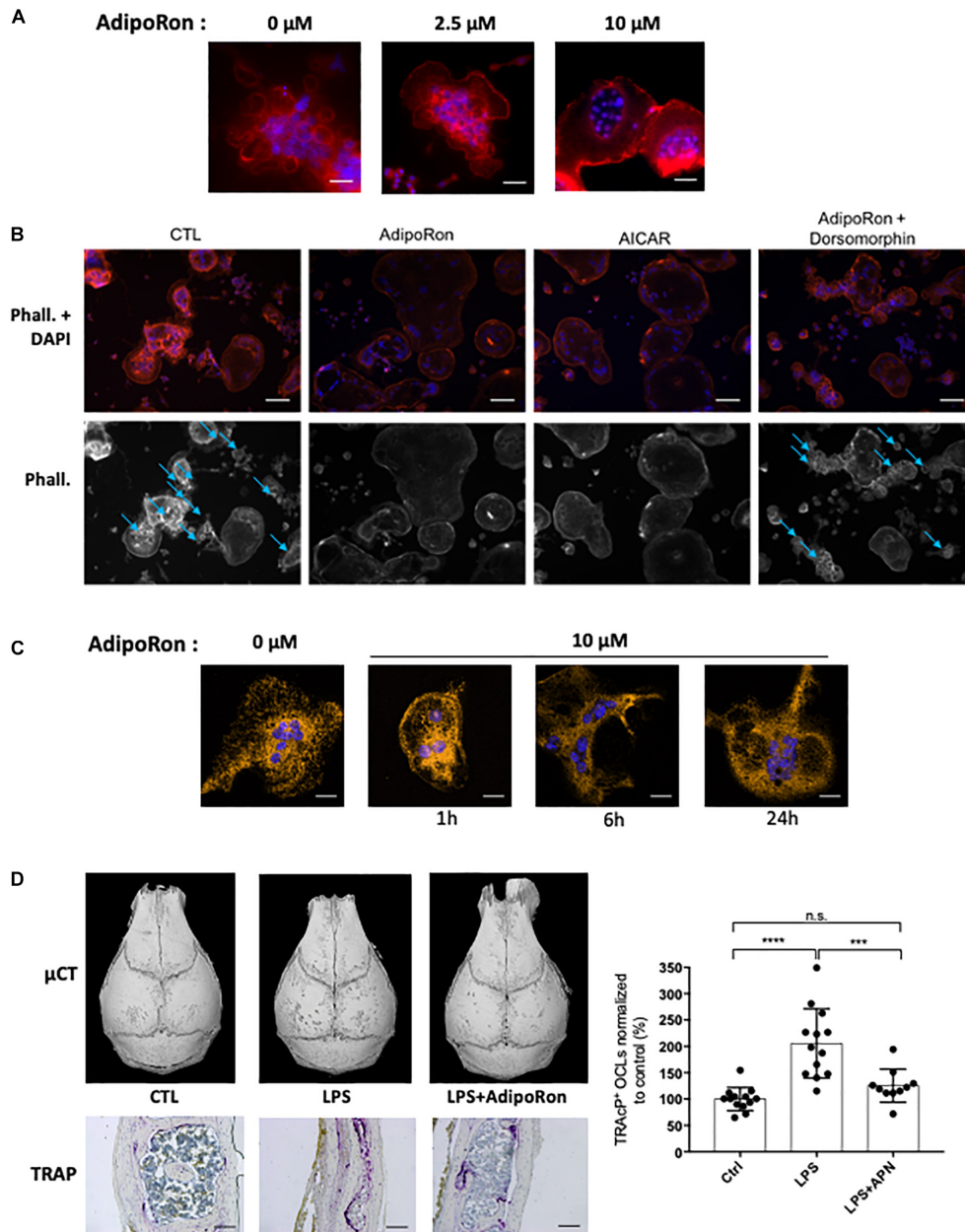


FIGURE 5 | Adiponectin regulates OCL activity and podosome formation. **(A)** Confocal microscopy of phalloidin-marked podosomes in RAW264.7-OCL in the presence of increasing concentrations of AdipoRon (representative images of $n = 3$ per concentration) Scale bars = 100 μ m. **(B)** Confocal microscopy of phalloidin-marked podosomes in the presence of AMPK modulating drugs (AdipoRon, 10 μ M; AICAR, 50 nM; Dorsomorphin, 1.2 μ M) (representative image of $n = 3$ per conditions white asterisks marking the podosomes). Scale bars = 50 μ m. Blue arrows indicate podosome rings. **(C)** Confocal microscopy of MitoTracker Orange in mature RAW264.7-OCL after AdipoRon (10 μ M) challenge at different time points. Scale bars = 20 μ m. **(D)** Mice received daily s.c. injections on the calvaria. Mice were injected with either 100 μ g lipopolysaccharide from *Salmonella abortus equi* (LPS), or 100 μ g LPS + 500 ng AdipoRon (LPS + AdipoRon) or vehicle (PBS) injection (control, CTL). Mouse skulls were collected on the 3rd day ($n = 3$ animals per group); Top panels: Micro-CT of the mouse skulls; Bottom panels: TRAcP staining of mouse skull after LPS +/- AdipoRon challenge, (representative sections from 3 animals per group), scale bars = 100 μ m. Right panel: quantification of the TRAcP staining. Two-group comparisons were performed using the Student's t-test. *** $p < 0.001$, **** $p < 0.0001$.

obtained with mouse cells, low dose of AdipoRon significantly inhibited RANKL-induced human osteoclast differentiation (**Supplementary Figures S5A,B**). AdipoRon also activated AMPK phosphorylation in human PBMC-derived osteoclasts

within minutes (**Supplementary Figure S5C**). At later time-point, i.e., within hours after the challenge with AdipoRon, the number of actin-containing podosome was drastically reduced in human osteoclasts (**Supplementary Figure S5D**).

These original findings offer new therapeutic perspectives in inflammatory bone loss management by targeting adiponectin/AdipoR.

DISCUSSION

In the present report, using lipodystrophic mouse models, we evaluated how the total lack of adipose tissue may affect bone homeostasis. Taken together our results demonstrate that mature osteoclasts are sensitive to extrinsic adipose-derived metabolic signals such as adipokine and that bone marrow adiposity must be considered as a physiological regulator of bone homeostasis. Consistently with the literature, we identified adiponectin as one main inhibitory signal for osteoclastogenesis. Herein, we further showed that AdipoRon, a pharmacological agonist of adiponectin receptors, inhibits osteoclast differentiation of precursors from different origins (bone marrow, dendritic and monocytic cells). We also demonstrated that adiponectin signaling inhibits human osteoclast differentiation as well as activity of human mature osteoclast and explored how AMPK signaling act on mature osteoclast activity via podosome formation blockade. These original findings reveal a conserved adiponectin-mediated metabolic control of osteoclast activity and are clinically promising, in particular with regard to the treatment and prevention of excessive pathological bone-resorption conditions, such as in osteoporotic patients.

The first model used in the present study, the *Pparγ* null mice, is bringing up some decisive arguments with respect to the controversy on the role of PPAR γ in osteoclastogenesis. Whereas initial studies reported that PPAR γ is a key factor for osteoclastogenesis (Wan et al., 2007), they could not confirm such activity and proposed that only pharmacological activation of PPAR γ had impact on osteoclastogenesis (Zou et al., 2016). Herein, we definitely demonstrate that osteoclastogenesis can occur in the absence of PPAR γ signal, and that other adipose tissue-derived signals, such as adipokines, affect osteoclast differentiation and activity. In contrast, the increase trabecular bone formation seen in vertebrae, in femoral epiphyses and distal diaphysis of *Pparg Δ/Δ* mouse is consistent with the known role of PPAR γ in inhibiting osteogenesis.

Using three complementary genetic models (2 distinct conditional null mice of *Pparγ* and the *AZIP^{tg/+}* mice, a PPAR γ -independent lipoatrophy model), we showed that the dramatic cortical bone alteration due to an excessive osteoclastogenesis in mice is linked to the lack of adipocyte and adipocyte-derived signals. The systemic and local activities of adipokines such as leptin and adiponectin have been recently reviewed (Cornish et al., 2018). Although leptin can act as a positive regulator of osteogenesis in *in vitro* systems, other studies in mice show that systemic leptin acting via the central nervous system is a potent inhibitor of bone formation (Ducy et al., 2000). Systemic adiponectin was reported to promote bone formation through its depressive action on the sympathetic tone in mice in age-dependent manner (Kajimura et al., 2013). However, *in vitro* differentiation assay showed that adiponectin inhibits osteoclast formation (Oshima et al., 2005;

Yamaguchi et al., 2008). The observations *in vivo* are more controversial. Adiponectin-null mice exhibit an increased trabecular volume and fewer osteoclasts according to Wang et al. (2014), whereas Shinoda et al. (2006) found normal bone development in these mice. In contrast, Naot et al. (2016) described a decreased cortical thickness in adiponectin-null female mice and Yang et al. (2019) a decreased bone mass. Interestingly, the female bias of the phenotype observed herein was also found in adiponectin-null mice. Thus, adiponectin may have different effects on bone remodeling, depending on the activated autocrine, paracrine or systemic pathways (Tu et al., 2011). Our results from the osteoclastogenesis assay using bone marrow-derived cells and adiponectin-specific blocking antibodies support the important paracrine role of adiponectin in the inhibition of osteoclastogenesis in the normal BM environment. Direct paracrine activity is also consistent with the presence of the adiponectin receptors, AdipoR1 and AdipoR2, on the surface of differentiating osteoclasts (Pacheco-Pantoja et al., 2013). Nonetheless, we cannot exclude that other adipokines may also contribute to the paracrine effects of adipocytes on osteoclasts.

Identifying the source of adiponectin in the vicinity of osteoclast precursors and/or mature osteoclasts in bone marrow and bone compartment is challenging. Indeed, levels of adiponectin production by BM adipocytes remain controversial. Cawthorn et al. (2014) reported that BM adipocytes serve as a major source of circulating adiponectin exerting systemic effects during caloric restriction whereas others groups reported that bone marrow adipocytes express lower levels of adiponectin than adipocytes in adipose tissue (Liu et al., 2011; Poloni et al., 2013; Li et al., 2019). Other sources of bone marrow adiponectin have been recently described. Bone marrow PDGFR β^+ VCAM-1 $^+$ stromal cells have been identified as major producers of adiponectin in the bone marrow (Mukohira et al., 2019). Single cell transcriptomic profiling of the mouse bone marrow stromal compartment indicated that LepR $^+$ bone marrow mesenchymal stromal cells, which form a functional continuum with osteolineage cells, are expressing adiponectin (Baryawno et al., 2019). Beside their proliferative action on HSC and antiproliferative effects on myelomonocytic and early B lymphoid cells, these adiponectin-producing cells appears to be essential to the hematopoietic niche. In this context, our finding that adiponectin regulates osteoclast activity and differentiation in bone further strengthens the argument that a metabolic pathway driven by adiponectin controls many osteoimmunology processes, including remodeling of bone marrow hematopoietic stem cell niche, with potential implications for multiple human disease states including cancer.

The distinct behavior and response of trabecular bone versus cortical bone is particularly highlighted in *Pparg Δ/Δ* mice. Such contrasting phenotype has been previously observed. For example, increased or decreased mechanical strain (Ausk et al., 2013) or fluoride treatment increase the density of trabecular bone but decrease the density of cortical bone (Connett, Fluoride Action network, April 2012)¹. This bivalent phenotype

¹<http://fluoridealert.org/studies/bone03/>

is reminiscent of that observed when osteoblast and osteocyte apoptosis is prevented via targeted deletion of the proapoptotic proteins Bak/Bax (Jilka et al., 2014). In this context, a severe increase in cortical porosity was accompanied by increased osteoclast formation. The prolonged lifespan of osteoblasts was proposed by the authors to trigger diametrically opposed biological effects on bone homeostasis with an exaggeration of the adverse effects of aging due to long-lived osteocytes (Jilka et al., 2014). In particular, osteocytes may increase intracortical remodeling via their secretion of RANKL and the subsequent activation of osteoclasts (Fuller et al., 1998; Jilka et al., 2014; Rinotas et al., 2014). In *Pparg*^{Δ/Δ} mice, the levels of *Sost* and *Keratocan* gene expression as markers of osteocytes and osteoblasts, respectively, are unchanged with respect to those found in their control littermates, thus refuting the possibility of an increased number of both cell types. In parallel, the increased expression of *Ctsk* and *Mmp9* likely contributes to the loss of cortical bone owing to high osteoclast activity, whereas the well-established role of PPAR γ deficiency in bone formation via osteoblast activation is particularly highlighted by the increased trabecular bone density. Finally, it has been recently shown that osteoclasts have some site-dependent specificities and heterogeneity (Madel et al., 2019), that could contribute to the distinct behavior of the cortical bone vs. trabecular bone.

The difference in the intensity of the cortical porosity observed between the three lipodystrophic models we used may stem from different causes. On the one hand, the fact that the phenotype is more marked in the *Pparg*^{Δ/Δ} mice indicates that the expression of PPAR γ in other cell types including osteoblasts and osteoclasts may dampen the phenotype in the AZIP and in the *Pparg*^{adipoKO} models, irrespectively of adiponectin signals. However, a clear contribution of adipocytes remains highlighted by the results in AZIP mice which expressed functional PPAR γ in all cell types. On the other hand, adiponectin gene expression, barely detectable in *Pparg*^{Δ/Δ} mice, is still present in the AZIP model and could contribute to the difference of phenotype penetrance between these two mouse models.

One important finding of the present report is the mechanism by which AdipoR signaling affects osteoclast activity. Indeed, here we demonstrated that AMPK was activated following AdipoRon challenge, which resulted in alteration of osteoclast metabolism, as exemplified by the alteration of the perinuclear mitochondrial network. We cannot exclude that direct or indirect signaling events may occur following adipoRon challenge that could interfere with osteoclast activity genetic program, such as Akt or NFATc1 signaling pathway as previously demonstrated with recombinant adiponectin (Yamaguchi et al., 2008; Tu et al., 2011). However, AMPK is central in this process, since its activation induced mitochondrial network alteration and podosome formation blockade, whereas AMPK blockade reverted these effects. Similarly, we also demonstrated that adiponectin signaling inhibits human osteoclast differentiation as well as activity of human mature osteoclast.

Altogether, these original findings reveal a conserved adiponectin-mediated metabolic control of osteoclast activity and are clinically promising, in particular with regard to the treatment and prevention of excessive pathological

bone-resorption conditions, such as in osteoporotic patients. The present study implies that preserving functional adiponectin sensitivity in patients suffering from metabolic diseases (e.g., diabetes, obesity, metabolic syndrome) might be also beneficial for preventing bone fragility.

MATERIALS AND METHODS

Key Resources Table

Reagent or resource	Source	Identifier
Antibodies		
Neutralizing adiponectin receptor 1 polyclonal antibody	Enzo life science	ALX-210-645-C200
Adiponectin rabbit monoclonal antibody	Cell signaling technology	#2789
AMPK(Rabbit mAb (D63G4)	Cell signaling technology	#5832
Phospho-AMPK α (Thr172) (40H9) Rabbit mAb	Cell signaling technology	#2535
Chemicals, peptides, and recombinant proteins		
Fetal Bovine Serum	GIBCO	10082139
Alpha MEM with NTP, dNTP	GIBCO	22571
AdipoRon	SIGMA	SML0998
mRANKL	R&D systems	462-TEC
hRANKL	R&D systems	6449-TEC
Critical commercial assays		
Acid Phosphatase, Leukocyte (TRAP) assay	SIGMA	387A
murine serum CTX ELISA	LSBio	F21349
murine serum OCN ELISA	LSBio	F12227
murine serum PTH ELISA	LSBio	F23085
Experimental models: cell lines		
3T3-L1 pre adipose murine cell line	ATCC	CL-173
RAW 264.7 murine macrophage	ATCC	TIB-71
Experimental models: organisms/strains		
Sox2-Cre mouse	The Jackson Laboratory	004783
Adipoq-Cre mouse	The Jackson Laboratory	010803
Ppar γ L2/L2 mouse	B Desvergne	
AZIP/F1 tg mouse	C Vinson	
Oligonucleotides (primers): see Supplementary Table 1		
Software and algorithms		
CTan CTVol	Skyscan	
ImageJ	Fiji	

Mouse Models

Genotype denomination follows the rules recommended by the Mouse Genome Database (MGD) Nomenclature Committee. Animal procedures were authorized by the Canton of Vaud veterinary service. Sox2CRE transgenic mice [SOX2CRE^{tg/+}; Tg(Sox2-cre)1Amc/J] and AdipoQCRE (*Adipoq-Cre*^{tg/+}) from The Jackson Laboratory, were maintained in the University of Lausanne Animal Facility. The series of matings allowing the

generation of the SOX2CRE^{tg/+}*Pparg*^{em Δ/Δ} mouse (hereafter called *Pparg* ^{Δ/Δ}), which expressed the SOX2CRE transgene and have no *Ppar γ* functional alleles, as well as their control littermates (CTL) that have no SOX2CRE transgene and two functional *Ppar γ* alleles (*Pparg*^{fl/+}) have been described in Gilardi et al. (2019). The resulting genetic background of these mice are a mix of C57Bl6 and SV129L. *Pparg*^{adipoKO} and their control littermates were generated as described in Wang et al. (2013), in a mixed genetic background C57Bl6 and SV129L. AZIP/F1 mice on FVB background [Tg(AZIP/F)1Vsn in MGD, herein called AZIP^{tg/+}] and wild type FVB controls were a kind gift from Dr. Charles Vinson and were generated as previously described (Moitra et al., 1998).

Primary Cell Culture

Mouse bone marrow cells were isolated by crushing entire long bones into DMEM/3% FCS (GIBCO). Bone fragments were removed by filtration through a 70 μ m filter mesh. Splenocyte suspensions were obtained by mashing the spleen through sieves into DMEM/3% FCS, washing by centrifugation then filtering through 70 μ m filter caps. Primary osteoblasts from neonatal calvaria of *Pparg*^{fl/+} and *Pparg* ^{Δ/Δ} were harvested by sequential collagenase type II (3 mg/mL) digestions of individual calvarium from 2 to 3-day-old mice. After genotyping, calvaria cells of the same genotype were pooled and plated accordingly. The cells were incubated at 37°C with 5% CO₂ and media was changed every 2 days until they reached 80% confluency. To assess proliferation, primary osteoblasts were plated in 24-well plates at a concentration of 10,000 cells/well in EMEM media (GIBCO) containing 10% FBS, 100 U/ml penicillin and 100 μ g/ml streptomycin (GIBCO).

Osteoclastogenesis Assays and TRAcP Staining of Murine and Human Primary Cells

Erythrocytes were eliminated from murine splenocyte and BM preparation or human PBMC using ACK lysis buffer. When indicated, osteoclasts were also derived from CD11b⁺ monocytic cells (MN-OCLs) and bone marrow-derived CD11c⁺ dendritic cells (DC-OCLs) as described previously (Ibáñez et al., 2016). Cells were cultured in complete α MEM with 40 ng/ml M-CSF (ProSpec-Tany TechnoGene, Rehovot, Israel) and 10 ng/ml RANKL (R&D Systems, MN). Tartrate-resistant acid phosphatase (TRAcP) staining was performed after 4–6 days, using the Acid Phosphatase, Leukocyte (TRAP) Kit according to the manufacturer's instructions (Sigma). Mature osteoclasts were identified as multi-nucleate TRAcP⁺ cells using light microscopy. 3T3-L1 cells (ATCC) were grown to sub-confluence in DMEM/10% FBS. Cells were then cultured in adipogenic conditions [DMEM/10%FBS, 0.5 mM 3-isobutyl-1-methylxanthine, 1 μ M dexamethasone (Sigma), and 10 μ g/ml bovine insulin (Sigma)] for 2 weeks, after which the medium was changed back to DMEM/10% FBS. Adipocyte Conditioned Medium (A-CM) was collected after 24 hours exposure to differentiated cells. Similarly, conditioned control medium (CTL) was obtained from undifferentiated

3T3-L1 cells. A-CM and CTL were concentrated 5X using CentriprepTM (Millipore). Conditioned medium from either differentiated or undifferentiated 3T3-L1 cells was added during osteoclastogenesis from multipotent progenitor cells. For neutralization experiments, 50% CM was incubated with different amounts of anti-adiponectin antibody (Enzo Life Sciences) for 30 min at room temperature then added during osteoclastogenesis. TRAcP staining to evaluate osteoclast numbers was performed as mentioned above.

Osteoclast Differentiation and TRAcP Staining of RAW 264.7 Cells

For osteoclastogenesis, a total of 1×10^4 RAW 264.7 (ATCC) cells were seeded per well on 24-well plates in 500 μ l α MEM containing 5% FCS (Hyclone, GE Healthcare), 1% penicillin-streptomycin (Gibco) as well as 50 μ M β -mercaptoethanol (Gibco) and 30 ng/ml murine RANKL (R&D Systems). To study the impact of adiporon on osteoclast differentiation, 10 μ M AdipoRon (Sigma-Aldrich) were added to the culture medium. Tartrate-resistant acid phosphatase (TRAcP) activity was examined using the leucocyte acid phosphatase kit (Sigma-Aldrich) according to manufacturer's specifications. TRAcP⁺ cells with ≥ 3 nuclei were considered as osteoclasts. In addition, 5×10^3 RAW 264.7 cells were seeded per well in a Nunc Lab-Tek II 8-well Chamber Slide system (ThermoFisher Scientific) in a total of 300 μ l osteoclast differentiation medium containing 30 ng/ml RANKL. Fully differentiated osteoclasts were treated with 10 μ M AdipoRon for the indicated time points. FACS analysis as well as sorting of mature OCLs for subsequent Western-blot analyses was performed as described previously (Madel et al., 2018).

Measurement of Bone Morphology and Microarchitecture

Unless otherwise indicated, 1-year old females of each genotype were used for bone analyses.

High-resolution micro-computed tomography (UCT40, ScancoMedical AG, Bassdorf, Switzerland) was used to scan the femur and the 5th lumbar vertebral body. Data were calibrated against a phantom, which has a known hydroxyapatite value. For the vertebral trabecular region, we evaluated ~ 300 transverse CT slices between the cranial and caudal end plates, excluding 100 μ m near each endplate. Femoral cortical geometry was assessed in a 1 mm-long region centered at the femoral midshaft. CT images were reconstructed in $1,024 \times 1,024$ pixel matrices using a standard convolution-backprojection procedure, and the resulting gray-scale images were segmented using a constrained 3D Gaussian filter ($\sigma = 0.8$, support = 1.0) to remove noise, and a fixed threshold (22 and 30% of maximal gray scale value for trabecular bone and cortical bone, respectively) was used to extract the structure of mineralized tissue.

Cortical and trabecular bones were evaluated using isotropic 12 μ m voxels. For trabecular bones, we assessed bone volume fraction (BV/TV,%), trabecular thickness (Tb.Th, μ m), trabecular number (Tb.N, mm⁻¹), and trabecular separation (Tb.Sp, μ m). For cortical midshaft femur, we measured the average total

volume (TV, mm³), bone volume (BV, mm³), and average cortical thickness (μm). SkyScan software (CTAn and CTVol) was employed to calculate cortical bone porosity of femur using a dedicated method after acquisition using a Skyscan 1272 (SkyScan 1272, Bruker, Brussels, Belgium) at a resolution of 10 μm/pix, and a threshold set up at 100–255, finally visualized in 3D.

Serum Protein Assays

Blood was obtained by cardiac puncture immediately after euthanasia. After clotting and centrifugation, serum was collected and stored at –80°C until use. Serum CTX (carboxy-terminal collagen crosslinks), osteocalcin (OCN), alkaline phosphatase (ALP), and parathyroid hormone (PTH) were measured by ELISA assays according to the manufacturer's protocol (LifeSpan Biosciences, Inc., Seattle, WA).

Calvaria Injection

Nine 6-week old C57/BL6 male mice were purchased from Envigo and housed in the local animal facility under a 12 h light/12 h dark cycle. The animals were randomly divided into three experimental groups, each group comprising three mice. Mice received daily *s.c.* injections on the calvaria before analysis on the third day. Group 1 was injected with 100 μg lipopolysaccharide from *Salmonella abortus equi* (LPS, Sigma-Aldrich), group 2 with 100 μg LPS + 500 ng AdipoRon (Sigma-Aldrich) and experimental group 3 underwent vehicle (PBS) injection. Calvariae were collected and fixed overnight in 4% formaldehyde at 4°C and then stored in 70% EtOH. Subsequent micro-CT analysis were used to evaluate the resorbed area. Calvariae were decalcified in 10% EDTA, embedded in paraffin and 5-micron sections were cut and stained for tartrate-resistant acid phosphatase (TRAcP, Sigma-Aldrich).

Quantitative RT-PCR

Total RNA was isolated from total long bones, including the crude BM, or primary cell cultures, using TRIzol LS (Invitrogen) and purified with the RNeasy kit (Qiagen). RNA quality was verified by microfluidic (Agilent 2100 Bioanalyzer) and concentration determined with a NanoDrop spectrophotometer (Wilmington). Total RNA (500 ng/μg) was reverse transcribed using ScriptTM cDNA synthesis kit (Bio-Rad) according to the manufacturer's instructions. Real time qPCR was performed with SYBR[®] Green PCR mastermix using an ABI PRISM[®] 7900 PCR machine (Applied Biosystems). Results were normalized to glyceraldehyde-3-phosphate dehydrogenase (*Gapdh*) or beta-actin beta (*Actb*). The primer sets are indicated in the **Supplementary Table S1**.

Western Blot Analysis

Mature OCLs were sorted based on their nuclei number (≥3) following the protocol described in Madel et al. (2018). This protocol ensures that further analyses (FACS and western-blot analysis) are made with a pure mature cell population, avoiding contaminant effects due to the important number of non-osteoclastic cells always present in classical culture, as reported (Madel et al., 2018). The sorted mature OCLs were washed

twice with ice-cold PBS and scraped in 1X Laemmli buffer. Cells were disrupted by sonication and centrifuged at 3,000 rpm for 10 min. Protein samples were analyzed by SDS/PAGE (gradient 4–15% acrylamide, Criterion, BioRad) and electroblotted onto 0.2% PVDF membrane using Transblot Turbo (BioRad). After 1 h in blocking buffer (Tris-buffered saline (TBS)–Tween 20 with 5% fat free dry milk), membranes were blotted overnight at 4°C with Rabbit mAb against AMPKα (D63G4) (dilution 1:1,000, Cell Signaling Technology) or Phospho-AMPKα (Thr172) (40H9) (dilution 1:1,000, Cell Signaling Technology), diluted in TBS–Tween with 5% BSA. After three washing steps with TBS–Tween 20, blot was incubated for 1 h at room temperature with anti-rabbit IgG conjugated with horseradish peroxidase diluted 1:2,000 in blocking buffer. After four additional washing steps with TBS–Tween 20, protein bands were detected by chemiluminescence using Chemi Doc XRS + (BioRad).

Imaging

Podosomes were visualized by phalloidin staining (Sigma-Aldrich) following manufacturer's instructions. After removing unbound phalloidin conjugates, cells were labeled with 1 μg/ml DAPI (Sigma-Aldrich). Microscopic imaging was performed using a fluorescence microscope (Zeiss Axio Observer D1). For mitochondrial analysis, live cells were labeled with 200 nM MitoTracker Orange (ThermoFisher) according to manufacturer's recommendations. After staining, cells were fixed in 4% formaldehyde, labeled with 1 μg/ml DAPI and subjected to z-stack confocal microscopy analyses (Zeiss LSM 710 on an inverted Axio Observer.Z1 stand). Images were processed using Fiji/Image J software (Schindelin et al., 2012).

Statistical Analysis

The data were analyzed using one- or two-factor ANOVA for multiple comparisons as appropriate. Two-group comparisons were performed using the Student's *t*-test. ns: non-significant, **p* < 0.05, ***p* < 0.01, ****p* < 0.001, *****p* < 0.0001.

DATA AVAILABILITY STATEMENT

The original contributions presented in the study are included in the article/**Supplementary Material**, further inquiries can be directed to the corresponding author/s.

ETHICS STATEMENT

The animal study was reviewed and approved by the Canton of Vaud Veterinary Service.

AUTHOR CONTRIBUTIONS

HF designed the experimental plan, performed the experiments, analyzed the data, and contribute to the original draft preparation. M-BM, DP, MS, CW, AW, CP, MT, and BT performed experiments, analyzed the data, and prepared the visualization. J-YJ, FG, SE, NB, and CB-W contributed to the

conceptualization, analyzed the data, and reviewed/edited the manuscript. BD and DM conceived the study, designed the experimental plan, supervised the study, analyzed the data, wrote the manuscript, and acquired financial support for the project, were the guarantors of this work and, as such, had full access to all the data in the study and take responsibility for the integrity of the data and the accuracy of the data analyses. All authors read and edited the manuscript.

FUNDING

This work was supported by the Etat de Vaud (BD and AW) the FNRS 31003A-135583/1 (BD), the Région Grand Est (J-Y), the Fondation Arthritis (DM), the French PIA project Lorraine Université d'Excellence, reference ANR-15-IDEX-04-LUE (J-Y and DM) and the Fondation pour la Recherche Médicale (FRM, ECO20160736019) (M-BM).

ACKNOWLEDGMENTS

We would like to acknowledge the Montpellier preclinical platform of ECELLFRANCE for the μ CT analysis (IRMB, Montpellier, France) and the microCT platform SC3M from the RMeS Lab, INSERM UMRS 1229 (Nantes, France).

SUPPLEMENTARY MATERIAL

The Supplementary Material for this article can be found online at: <https://www.frontiersin.org/articles/10.3389/fcell.2021.627153/full#supplementary-material>

Supplementary Video 1 | Video of 3D micro-CT reconstruction of genetically induced lipotrophic mice showing alterations of both trabecular and cortical femoral bone.

REFERENCES

- Akune, T., Ohba, S., Kamekura, S., Yamaguchi, M., Chung, U.-I., Kubota, N., et al. (2004). PPAR γ insufficiency enhances osteogenesis through osteoblast formation from bone marrow progenitors. *J. Clin. Invest.* 113, 846–855. doi: 10.1172/jci200419900
- Ali, A. A., Weinstein, R. S., Stewart, S. A., Parfitt, A. M., Manolagas, S. C., and Jilka, R. L. (2005). Rosiglitazone causes bone loss in mice by suppressing osteoblast differentiation and bone formation. *Endocrinology* 146, 1226–1235. doi: 10.1210/en.2004-0735
- Ausk, B. J., Huber, P., Srinivasan, S., Bain, S. D., Kwon, R. Y., McNamara, E. A., et al. (2013). Metaphyseal and diaphyseal bone loss in the tibia following transient muscle paralysis are spatiotemporally distinct resorption events. *Bone* 57, 413–422. doi: 10.1016/j.bone.2013.09.009
- Barak, Y., Nelson, M. C., Ong, E. S., Jones, Y. Z., Ruiz-Lozano, P., Chien, K. R., et al. (1999). PPAR γ is required for placental, cardiac, and adipose tissue development. *Mol. Cell* 4, 585–595. doi: 10.1016/s1097-2765(00)80209-9
- Baryawno, N., Przybylski, D., Kowalczyk, M. S., Kfoury, Y., Severe, N., Gustafsson, K., et al. (2019). A cellular taxonomy of the bone marrow stroma in homeostasis and leukemia. *Cell* 177, 1915–1932.e16.
- Calo, E., Quintero-Estades, J. A., Danielian, P. S., Nedelcu, S., Berman, S. D., and Lees, J. A. (2010). Rb regulates fate choice and lineage commitment in vivo. *Nature* 466, 1110–1114. doi: 10.1038/nature09264

Supplementary Figure 1 | Osteoblastic activity is increased in mice with epiblastic deletion of PPAR γ . (A) Representative 3-D micro-CT of the fourth lumbar vertebrae of CTL and *Pparg* Δ/Δ ($\gamma^{\Delta/\Delta}$) mice. $n = 5$ WT and 5 $\gamma^{\Delta/\Delta}$. (B) Trabecular bone volume fraction measured by micro-CT analysis of vertebra from $\gamma^{\Delta/\Delta}$ ($n = 5$) and control (CTL; $n = 5$) littermates. (C) Trabecular connectivity density measured by micro-CT analysis of vertebra from $\gamma^{\Delta/\Delta}$ ($n = 5$) and control (CTL; $n = 5$) littermates. (D) *Keratocan* and *Sost* mRNA levels in long bones of CTL ($n = 6$) and $\gamma^{\Delta/\Delta}$ ($n = 6$) mice.

Supplementary Figure 2 | Parathyroid hormone (PTH) signaling. The serum levels of PTH were assessed by Elisa Assay in 1-year-old male and female mice (*Pparg* Δ/Δ , *AZIP* $^{tg/+}$, and their control littermates). Six males and six females were included per genotype. As there were no statistically significant differences between males and females, the analysis was performed using the total number of mice (mean \pm SD). Lower panels: mRNA expression levels of *Pth1r* in the bones and in the kidneys of CTL vs. *Pparg* Δ/Δ mice.

Supplementary Figure 3 | Adiponectin expression levels in long bone and in adipocyte-conditioned medium. RT-qPCR analysis of *Leptin* and *AdipoQ* mRNA levels in long bone from A-ZIP $^{tg/+}$ ($n = 8$) and their CTL littermates ($n = 8$) and from $\gamma^{\Delta/\Delta}$ ($n = 7$) and their CTL littermates ($n = 6$). Data are presented as mean \pm S.E.M. Statistical significance was determined by two-tailed unpaired t-test.

Supplementary Figure 4 | AdipoRon inhibits osteoclast (OCL) differentiation of various origins. Left panels: representative images of TRAcP stained (A) BM-derived, (B) spleen derived, and (C) macrophages enriched fraction osteoclasts differentiated in the presence or absence of AdipoRon (5 μ M). Right panels: the mean IC50 of AdipoRon inhibition of OCL differentiation was determined from the curve with the error of the fit (S.E.M.) Data are mean \pm S.E.M. ($n = 3$ biological replicates).

Supplementary Figure 5 | AdipoRon inhibits human osteoclast (OCL) differentiation and activity through AMPK activation. (A) Dose response effect of AdipoRon on osteoclast differentiation from hPBMC ($n = 5$). (B) Representative images of TRAcP staining of hPBMC derived osteoclast differentiation in the presence or absence of AdipoRon (5 μ M). (C) Western-blot analysis of hPBMC-derived osteoclasts treated with AdipoRon (5 μ M). AdipoRon treatment activates AMPK phosphorylation (p-AMPK) in hPBMC after 5 min. (D) Fluorescence microscopy of phalloidin-marked podosomes in hPBMC derived OCL in the presence of AdipoRon (5 μ M, 12 h) (representative images of $n = 5$).

Supplementary Table 1 | Primers used for q-RT-PCR.

- Cawthorn, W. P., Scheller, E. L., Learman, B. S., Parlee, S. D., Simon, B. R., Mori, H., et al. (2014). Bone marrow adipose tissue is an endocrine organ that contributes to increased circulating adiponectin during caloric restriction. *Cell Metab.* 20, 368–375. doi: 10.1016/j.cmet.2014.06.003
- Chen, G., Huang, L., Wu, X., Liu, X., Xu, Q., Li, F., et al. (2018). Adiponectin inhibits osteoclastogenesis by suppressing NF- κ B and p38 signaling pathways. *Biochem. Biophys. Res. Commun.* 503, 2075–2082. doi: 10.1016/j.bbrc.2018.07.162
- Cornish, J., Wang, T., and Lin, J.-M. (2018). Role of marrow adipocytes in regulation of energy metabolism and bone homeostasis. *Curr. Osteoporos. Rep.* 16, 116–122. doi: 10.1007/s11914-018-0425-0
- Ducy, P., Amling, M., Takeda, S., Priemel, M., Schilling, A. F., Beil, F. T., et al. (2000). Leptin inhibits bone formation through a hypothalamic relay: a central control of bone mass. *Cell* 100, 197–207. doi: 10.1016/s0092-8674(00)81558-5
- Engsig, M. T., Chen, Q. J., Vu, T. H., Pedersen, A. C., Therkidsen, B., Lund, L. R., et al. (2000). Matrix metalloproteinase 9 and vascular endothelial growth factor are essential for osteoclast recruitment into developing long bones. *J. Cell Biol.* 151, 879–889. doi: 10.1083/jcb.151.4.879
- Felson, D. T., Zhang, Y., Hannan, M. T., and Anderson, J. J. (1993). Effects of weight and body mass index on bone mineral density in men and women: the framingham study. *J. Bone Miner. Res.* 8, 567–573. doi: 10.1002/jbmr.5650080507

- Fuller, K., Wong, B., Fox, S., Choi, Y., and Chambers, T. J. (1998). TRANCE is necessary and sufficient for osteoblast-mediated activation of bone resorption in osteoclasts. *J. Exp. Med.* 188, 997–1001. doi: 10.1084/jem.188.5.997
- Gilardi, F., Winkler, C., Quignodon, L., Diserens, J.-G., Toffoli, B., Schiffrin, M., et al. (2019). Systemic PPAR(deletion in mice provokes lipotrophy, organomegaly, severe type 2 diabetes and metabolic inflexibility. *Metab. Clin. Exp.* 95, 8–20. doi: 10.1016/j.metabol.2019.03.003
- Grey, A. (2008). Skeletal consequences of thiazolidinedione therapy. *Osteoporos. Int.* 19, 129–137. doi: 10.1007/s00198-007-0477-y
- Horowitz, M. C., Berry, R., Holtrup, B., Sebo, Z., Nelson, T., Fretz, J. A., et al. (2017). Bone marrow adipocytes. *Adipocyte* 6, 193–204.
- Ibáñez, L., Abou-Ezzi, G., Ciucci, T., Amiot, V., Belaid, N., Obino, D., et al. (2016). Inflammatory osteoclasts prime TNF(-producing CD4(T cells and express CX3CR1. *J. Bone Miner. Res.* 31, 1899–1908. doi: 10.1002/jbmr.2868
- Idris, A. I., Sophocleous, A., Landao-Bassonga, E., Canals, M., Milligan, G., Baker, D., et al. (2009). Cannabinoid receptor type 1 protects against age-related osteoporosis by regulating osteoblast and adipocyte differentiation in marrow stromal cells. *Cell Metab.* 10, 139–147. doi: 10.1016/j.cmet.2009.07.006
- Imai, T., Takakuwa, R., Marchand, S., Dentz, E., Bornert, J.-M., Messaddeq, N., et al. (2004). Peroxisome proliferator-activated receptor gamma is required in mature white and brown adipocytes for their survival in the mouse. *Proc. Natl. Acad. Sci. U.S.A.* 101, 4543–4547. doi: 10.1073/pnas.0400356101
- Iwabu, M., Yamauchi, T., Okada-Iwabu, M., Sato, K., Nakagawa, T., Funata, M., et al. (2010). Adiponectin and AdipoR1 regulate PGC-1alpha and mitochondria by Ca(2+) and AMPK/SIRT1. *Nature* 464, 1313–1319. doi: 10.1038/nature08991
- Iwaki, M., Matsuda, M., Maeda, N., Funahashi, T., Matsuzawa, Y., Makishima, M., et al. (2003). Induction of adiponectin, a fat-derived antidiabetic and antiatherogenic factor, by nuclear receptors. *Diabetes* 52, 1655–1663. doi: 10.2337/diabetes.52.7.1655
- Jemtland, R., Lee, K., and Segre, G. V. (1998). Heterogeneity among cells that express osteoclast-associated genes in developing bone. *Endocrinology* 139, 340–349. doi: 10.1210/endo.139.1.5664
- Jilka, R. L., O'Brien, C. A., Roberson, P. K., Bonewald, L. F., Weinstein, R. S., and Manolagas, S. C. (2014). Dysapoptosis of osteoblasts and osteocytes increases cancellous bone formation but exaggerates cortical porosity with age. *J. Bone Miner. Res.* 29, 103–117. doi: 10.1002/jbmr.2007
- Kahn, S. E., Zinman, B., Lachin, J. M., Haffner, S. M., Herman, W. H., Holman, R. R., et al. (2008). Rosiglitazone-associated fractures in type 2 diabetes: an analysis from a diabetes outcome progression trial (ADOPT). *Diabetes Care* 31, 845–851. doi: 10.2337/dc07-2270
- Kajimura, D., Lee, H. W., Riley, K. J., Arteaga-Solis, E., Ferron, M., Zhou, B., et al. (2013). Adiponectin regulates bone mass via opposite central and peripheral mechanisms through FoxO1. *Cell Metab.* 17, 901–915. doi: 10.1016/j.cmet.2013.04.009
- Kawai, M., and Rosen, C. J. (2010). PPAR: a circadian transcription factor in adipogenesis and osteogenesis. *Nat. Rev. Endocrinol.* 6, 629–636. doi: 10.1038/nrendo.2010.155
- Lazarenko, O. P., Rzonca, S. O., Hogue, W. R., Swain, F. L., Suva, L. J., and Lecka-Czernik, B. (2007). Rosiglitazone induces decreases in bone mass and strength that are reminiscent of aged bone. *Endocrinology* 148, 2669–2680. doi: 10.1210/en.2006-1587
- Levin, A., Bakris, G. L., Molitch, M., Smulders, M., Tian, J., Williams, L. A., et al. (2007). Prevalence of abnormal serum vitamin D, PTH, calcium, and phosphorus in patients with chronic kidney disease: results of the study to evaluate early kidney disease. *Kidney Int.* 71, 31–38. doi: 10.1038/sj.ki.5002009
- Li, Y., Meng, Y., and Yu, X. (2019). The unique metabolic characteristics of bone marrow adipose tissue. *Front. Endocrinol.* 10:69. doi: 10.1016/j.front.2018.01.009
- Liu, L.-F., Shen, W.-J., Ueno, M., Patel, S., and Kraemer, F. B. (2011). Characterization of age-related gene expression profiling in bone marrow and epididymal adipocytes. *BMC Genomics* 12:212.
- Madel, M.-B., Ibáñez, L., Rouleau, M., Wakkach, A., and Blin-Wakkach, C. (2018). A novel reliable and efficient procedure for purification of mature osteoclasts allowing functional assays in mouse cells. *Front. Immunol.* 9:2567.
- Madel, M.-B., Ibáñez, L., Wakkach, A., de Vries, T. J., Teti, A., Apparailly, F., et al. (2019). Immune function and diversity of osteoclasts in normal and pathological conditions. *Front. Immunol.* 10:1408.
- Moitra, J., Mason, M. M., Olive, M., Krylov, D., Gavrilo, O., Marcus-Samuels, B., et al. (1998). Life without white fat: a transgenic mouse. *Genes Dev.* 12, 3168–3181. doi: 10.1101/gad.12.20.3168
- Mukohira, H., Hara, T., Abe, S., Tani-ichi, S., Sehara-Fujisawa, A., Nagasawa, T., et al. (2019). Mesenchymal stromal cells in bone marrow express adiponectin and are efficiently targeted by an adiponectin promoter-driven cre transgene. *Int. Immunol.* 45, 1219–1213.
- Naot, D., Watson, M., Callon, K. E., Tuari, D., Musson, D. S., Choi, A. J., et al. (2016). Reduced bone density and cortical bone indices in female adiponectin-knockout mice. *Endocrinology* 157, 3550–3561. doi: 10.1210/en.2016-1059
- Okada-Iwabu, M., Yamauchi, T., Iwabu, M., Honma, T., Hamagami, K.-I., Matsuda, K., et al. (2013). A small-molecule AdipoR agonist for type 2 diabetes and short life in obesity. *Nature* 503, 493–499. doi: 10.1038/nature12656
- Oshima, K., Nampei, A., Matsuda, M., Iwaki, M., Fukuhara, A., Hashimoto, J., et al. (2005). Adiponectin increases bone mass by suppressing osteoclast and activating osteoblast. *Biochem. Biophys. Res. Commun.* 331, 520–526. doi: 10.1016/j.bbrc.2005.03.210
- Pacheco-Pantoja, E. L., Waring, V. J., Wilson, P. J. M., Fraser, W. D., and Gallagher, J. A. (2013). Adiponectin receptors are present in RANK-L-induced multinucleated osteoclast-like cells. *J. Recept. Signal Transduct. Res.* 33, 291–297. doi: 10.3109/10799893.2013.828070
- Poloni, A., Maurizi, G., Serrani, F., Mancini, S., Zingaretti, M. C., Frontini, A., et al. (2013). Molecular and functional characterization of human bone marrow adipocytes. *Exp. Hematol.* 41, 558–566.e2.
- Rinotas, V., Niti, A., Dacquin, R., Bonnet, N., Stolina, M., Han, C.-Y., et al. (2014). Novel genetic models of osteoporosis by overexpression of human RANKL in transgenic mice. *J. Bone Miner. Res.* 29, 1158–1169. doi: 10.1002/jbmr.2112
- Rosen, E. D., Sarraf, P., Troy, A. E., Bradwin, G., Moore, K., Milstone, D. S., et al. (1999). PPAR gamma is required for the differentiation of adipose tissue in vivo and in vitro. *Mol. Cell* 4, 611–617.
- Rzonca, S. O., Suva, L. J., Gaddy, D., Montague, D., and Lecka-Czernik, B. (2004). Bone is a target for the antidiabetic compound rosiglitazone. *Endocrinology* 145, 401–406. doi: 10.1210/en.2003-0746
- Sardella, C., Winkler, C., Quignodon, L., Hardman, J. A., Toffoli, B., Giordano Attianese, G. M. P., et al. (2018). Delayed hair follicle morphogenesis and hair follicle dystrophy in a lipotrophy mouse model of pparγ total deletion. *J. Invest. Dermatol.* 138, 500–510. doi: 10.1016/j.jid.2017.09.024
- Schindelin, J., Arganda-Carreras, I., Frise, E., Kaynig, V., Longair, M., Pietzsch, T., et al. (2012). Fiji: an open-source platform for biological-image analysis. *Nat. Methods* 9, 676–682. doi: 10.1038/nmeth.2019
- Sheu, Y., and Cauley, J. A. (2011). The role of bone marrow and visceral fat on bone metabolism. *Curr. Osteoporos. Rep.* 9, 67–75. doi: 10.1007/s11914-011-0051-6
- Shinoda, Y., Yamaguchi, M., Ogata, N., Akune, T., Kubota, N., Yamauchi, T., et al. (2006). Regulation of bone formation by adiponectin through autocrine/paracrine and endocrine pathways. *J. Cell. Biochem.* 99, 196–208. doi: 10.1002/jcb.20890
- Sun, H., Kim, J. K., Mortensen, R., Mutyaba, L. P., Hankenson, K. D., and Krebsbach, P. H. (2013). Osteoblast-Targeted suppression of PPAR(increases osteogenesis through activation of mTOR signaling. *Stem Cell* 31, 2183–2192. doi: 10.1002/stem.1455
- Takada, I., Kouzmenko, A. P., and Kato, S. (2009). Wnt and PPAR(signaling in osteoblastogenesis and adipogenesis. *Nat. Rev. Rheumatol.* 5, 442–447. doi: 10.1038/nrrheum.2009.137
- Toffoli, B., Gilardi, F., Winkler, C., Soderberg, M., Kowalczyk, L., Arsenijevic, Y., et al. (2017). Nephropathy in Pparg-null mice highlights PPAR(systemic activities in metabolism and in the immune system. *PLoS One* 12:e0171474. doi: 10.1371/journal.pone.0171474
- Tontonoz, P., and Spiegelman, B. M. (2008). Fat and beyond: the diverse biology of PPARgamma. *Annu. Rev. Biochem.* 77, 289–312. doi: 10.1146/annurev.biochem.77.061307.091829
- Tu, Q., Zhang, J., Dong, L. Q., Saunders, E., Luo, E., Tang, J., et al. (2011). Adiponectin inhibits osteoclastogenesis and bone resorption via APPL1-mediated suppression of Akt1. *J. Biol. Chem.* 286, 12542–12553. doi: 10.1074/jbc.m110.152405
- Wan, Y. (2010). PPAR in bone homeostasis. *Trends Endocrinol. Metab.* 21, 722–728.

- Wan, Y., Chong, L.-W., and Evans, R. M. (2007). PPAR-gamma regulates osteoclastogenesis in mice. *Nat. Med.* 13, 1496–1503. doi: 10.1038/nm1672
- Wang, F., Mullican, S. E., DiSpirito, J. R., and Peed, L. C. (2013). Lipoatrophy and severe metabolic disturbance in mice with fat-specific deletion of PPAR. *Proc. Natl. Acad. Sci. U.S.A.* 110, 18656–18661. doi: 10.1073/pnas.1314863110
- Wang, Q.-P., Li, X.-P., Wang, M., Zhao, L.-L., Li, H., Xie, H., et al. (2014). Adiponectin exerts its negative effect on bone metabolism via OPG/RANKL pathway: an in vivo study. *Endocrine* 47, 845–853. doi: 10.1007/s12020-014-0216-z
- Yamaguchi, N., Kukita, T., Li, Y.-J., Kamio, N., Fukumoto, S., Nonaka, K., et al. (2008). Adiponectin inhibits induction of TNF-alpha/RANKL-stimulated NFATc1 via the AMPK signaling. *FEBS Lett.* 582, 451–456. doi: 10.1016/j.febslet.2007.12.037
- Yang, J., Park, O.-J., Kim, J., Han, S., Yang, Y., Yun, C.-H., et al. (2019). Adiponectin deficiency triggers bone loss by up-regulation of osteoclastogenesis and down-regulation of osteoblastogenesis. *Front. Endocrinol.* 10:815.
- Zou, W., Rohatgi, N., Chen, T. H.-P., Schilling, J., Abu-amer, Y., and Teitelbaum, S. L. (2016). PPAR- regulates pharmacological but not physiological or pathological osteoclast formation. *Nat. Med.* 22, 1203–1205. doi: 10.1038/nm.4208

Conflict of Interest: The authors declare that the research was conducted in the absence of any commercial or financial relationships that could be construed as a potential conflict of interest.

Copyright © 2021 Madel, Fu, Pierroz, Schiffrin, Winkler, Wilson, Pochon, Toffoli, Taïeb, Jouzeau, Gilardi, Ferrari, Bonnet, Blin-Wakkach, Desvergne and Moulin. This is an open-access article distributed under the terms of the Creative Commons Attribution License (CC BY). The use, distribution or reproduction in other forums is permitted, provided the original author(s) and the copyright owner(s) are credited and that the original publication in this journal is cited, in accordance with accepted academic practice. No use, distribution or reproduction is permitted which does not comply with these terms.